Toward Mission-Critical ISAC: Reliable Energy-Aware Coordination in UAV Swarms

Masoud Shokrnezhad
ICTFICIAL Oy
Finland
masoud.shokrnezhad@ictficial.com

Tarik Taleb
Ruhr University Bochum
Germany
tarik.taleb@ruhr-uni-bochum.de

Amir Javadpour
ICTFICIAL Oy
Finland
amir.javadpour@ictficial.com

***Abstract*—Unmanned aerial vehicle (UAV) swarms deployed in mission-critical applications must simultaneously track a mobile aerial target and maintain reliable data links. However, active integrated sensing and communication (ISAC) operation imposes a dual energy burden on propulsion and transmission, threatening mission continuity through premature battery depletion. In this paper, we propose a two-tier UAV swarm architecture in which mission UAVs (MUAVs) execute cooperative ISAC for mobile aerial target tracking while dedicated charging UAVs (CUAVs), equipped with solar harvesting panels, replenish low-battery MUAVs via aerial UAV-to-UAV wireless power transfer (WPT). We formulate the joint minimization of the cooperative posterior Cramér–Rao bound (PCRB) over MUAV trajectories, per-slot sensing-communication time splits, WPT scheduling and admission, and CUAV rendezvous trajectories, subject to minimum uplink rate, dual-tier energy causality, WPT proximity, collision-avoidance, and speed constraints, yielding a non-convex mixed-integer program (MIP) that, to the best of our knowledge, is the first to jointly couple cooperative ISAC sensing quality with aerial WPT and dual-tier energy management. To solve it efficiently, we propose Receding-Horizon Alternating Optimization (RHAO), a four-block per-slot algorithm that decomposes the problem into: charging admission via the Hungarian algorithm, MUAV trajectory and time-split via successive convex approximation (SCA), CUAV rendezvous, and WPT power allocation, with monotone convergence guarantees. Simulation results demonstrate that RHAO reduces the mean PCRB by $16.8\times$ over a fixed-time-split baseline and $5.4\times$ over a static-trajectory scheme, while the aerial WPT subsystem sustains all MUAVs above the energy-critical threshold throughout the full mission horizon.**

***Index Terms*—integrated sensing and communication, UAV swarms, wireless power transfer, target tracking, energy management**

I. Introduction

Unmanned aerial vehicles (UAVs) are increasingly deployed in mission-critical applications (aerial surveillance, search-and-rescue, infrastructure inspection, and low-altitude logistics) where real-time situational awareness and reliable data connectivity must coexist. Integrated sensing and communication (ISAC) allows UAVs to share spectrum and hardware resources for simultaneous cooperative target tracking and telemetry relay, offering high spectral efficiency without dedicated sensing hardware. In a multi-UAV ISAC swarm, each agent contributes range measurements whose Fisher information combines cooperatively: geometric diversity across the swarm reduces the posterior Cramér–Rao bound (PCRB) on target state estimation far beyond what any single UAV can achieve, enabling precise tracking of highly dynamic aerial targets. However, active ISAC operation imposes a dual energy burden(propulsion for trajectory following and transmit power for both radar waveforms and uplink data relay) that accelerates battery depletion. Energy exhaustion forces a UAV to abort its mission or return to base, collapsing the cooperative sensing formation precisely when continuous coverage is most needed. Two-tier architectures in which dedicated charging UAVs (CUAVs) carrying solar energy-harvesting panels autonomously rendezvous with low-battery mission UAVs (MUAVs) and replenish them via aerial UAV-to-UAV (U2U) wireless power transfer (WPT) offer a principled remedy: mission continuity is sustained without any MUAV leaving the swarm. Yet, jointly optimizing cooperative ISAC trajectories, per-slot sensing-communication time splits, WPT admission and power scheduling, and dual-tier energy causality under a unified sensing-quality objective remains an open problem that is the focus of this paper.

Multi-UAV ISAC for aerial target tracking has attracted growing research attention. Yan *et al.* [1] proposed a system in which a ground base station (BS) and multiple UAVs cooperatively minimize the PCRB subject to per-UAV communication constraints, solving the joint trajectory–beamforming problem via a curriculum-guided heterogeneous-agent proximal policy optimization algorithm. Wang *et al.* [2] addressed the same PCRB minimization goal in the low-altitude economy by jointly optimizing UAV trajectories, bandwidth allocation, and UAV–BS association through an efficient iterative descent-direction scheme. Li *et al.* [3] studied cooperative ISAC for low-altitude networks with a dynamic time-division strategy, maximizing sum communication rate under a cumulative radar mutual-information constraint via alternating optimization and successive convex approximation (SCA). Feng *et al.* [4] combined ISAC waveforms with an extended Kalman filter (EKF) for 3D urban relay trajectory planning, using a deep Q-network to navigate building blockages and serve non-line-of-sight (LoS) users. None of these works models onboard battery dynamics or aerial WPT replenishment.

On the energy management side, Naoya *et al.* [5] studied multi-UAV data collection supported by a supply UAV that charges mission agents in flight via WPT, using simulated annealing and a genetic algorithm to maximize operational rounds. Zhang *et al.* [6] (eU2U) proposed energy-efficient U2U wireless charging and trajectory co-design for IoT data collection, minimizing total propulsion and chargingloss energy via a Fermat-point geometric heuristic. Mondal *et al.* [7] addressed risk-aware UAV–UGV cooperative routing under stochastic fuel consumption using an attention-guided reinforcement learning framework. Ye *et al.* [8], Gao *et al.* [9], and Farhoudi *et al.* [10], [11] examined multi-tier UAV edge computing systems under energy harvesting, using Lyapunov optimization and multi-agent reinforcement learning respectively to balance task delay against long-term energy stability. None of these works incorporates an ISAC sensing objective or PCRB metric.

Despite this progress, a fundamental gap persists across both research threads: ISAC-UAV works treat battery energy as unlimited, while WPT-assisted UAV works focus on data collection or computation without a cooperative sensing objective. To the best of our knowledge, no prior formulation simultaneously addresses cooperative ISAC trajectory design, per-UAV sensing-communication time splitting, aerial U2U WPT scheduling with per-slot admission, and dual-tier energy causality under a unified PCRB criterion. The **contributions** of this paper are:

(i) We introduce a **two-tier swarm architecture** in which MUAVs execute cooperative ISAC for mobile aerial target tracking while solar-equipped CUAVs sustain their operation via on-demand aerial WPT.

(ii) We formulate the joint optimization of MUAV trajectories, sensing-communication time splits, U2U WPT scheduling and admission, and CUAV rendezvous trajectories under a cooperative PCRB minimization objective, yielding a non-convex mixed-integer program (MIP) that jointly couples ISAC sensing quality with dual-tier energy causality.

(iii) We propose **RHAO** (Receding-Horizon alternating optimization (AO)), which decomposes the MIP into per-slot subproblems (charging admission, MUAV trajectory and time-split, CUAV rendezvous, and WPT power allocation) with a monotone convergence guarantee.

The remainder is as follows. Section II presents the system and formulates the problem. Section III describes RHAO. Section IV reports simulation results. Section V concludes.

II. System Model and Problem Formulation

A. Network Architecture

We consider a two-tier UAV swarm comprising N *MUAVs*, indexed by $\mathcal{N} = \{1, \ldots, N\}$, and M *CUAVs*, indexed by $\mathcal{M} = \{1, \ldots, M\}$. The swarm operates cooperatively with a fixed ground BS at $\mathbf{q}_{\text{bs}} \in \mathbb{R}^3$ to track a mobile aerial target. The mission horizon is discretized into T slots of duration τ [s], with $\mathbf{q}_n[t] \in \mathbb{R}^3$ and $\mathbf{u}_m[t] \in \mathbb{R}^3$ denoting the 3D positions of MUAV n and CUAV m at slot t, respectively. MUAVs execute a cooperative ISAC mission: they transmit an ISAC waveform to collect range measurements of a target and relay the resulting sensing/telemetry data to the BS. CUAVs carry solar energy harvesting panels; when a MUAV's state of charge (SoC) falls below a safe level, a CUAV rendezvous with it and delivers energy via aerial WPT. Fig. 1 illustrates the two-tier architecture.

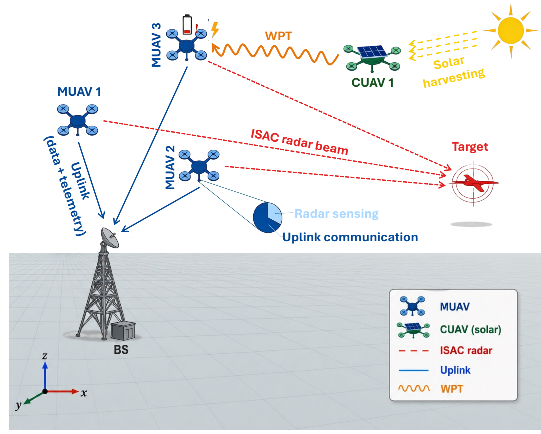

Fig. 1. Two-tier UAV swarm architecture. MUAVs (blue) perform cooperative ISAC: they transmit radar waveforms toward the mobile target and relay sensing data to the BS via uplink. CUAVs (green) carry solar harvesting panels and recharge low-battery MUAVs via aerial WPT.

B. ISAC Sensing and Communication Model

1) Target Dynamics: The target state at slot t is $\boldsymbol{\zeta}[t] = \left[\boldsymbol{\xi}[t]^T,\ \dot{\boldsymbol{\xi}}[t]^T\right]^T \in \mathbb{R}^6$, where $\boldsymbol{\xi}[t] = [x_t, y_t, z_t]^T$ is the 3D target position and $\dot{\boldsymbol{\xi}}[t] = [\dot{x}_t, \dot{y}_t, \dot{z}_t]^T$ is the corresponding velocity. Under a near-constant-velocity model over slot duration τ:

$$\boldsymbol{\zeta}[t] = \mathbf{F}\,\boldsymbol{\zeta}[t-1] + \boldsymbol{\varpi}[t-1], \quad \mathbf{F} = \mathbf{I}_3 \otimes \begin{bmatrix} 1 & \tau \\ 0 & 1 \end{bmatrix}, \tag{1}$$

where process noise $\boldsymbol{\varpi}[t] \sim \mathcal{N}(\mathbf{0}, \mathbf{Q})$, with $\mathbf{Q} \in \mathbb{R}^{6\times 6}$ denoting the process-noise covariance matrix that captures target maneuver uncertainty between slots.

2) Sensing-Communication Time Split: Each slot, MUAV n allocates fraction $\delta_n[t] \in [0, 1]$ to radar sensing and the complementary fraction $(1 - \delta_n[t])$ to uplink communication with the BS; both phases use transmit power P_n^{tx}.

3) Radar Measurement Model: MUAV n performs monostatic range sensing of the target. Let $d_n[t] = \|\mathbf{q}_n[t] - \boldsymbol{\xi}[t]\|$ denote the true MUAV–target range at slot t. The noise variance of the corresponding range measurement, derived from the radar range equation [1], is:

$$\sigma_n^2[t] = \frac{\kappa_s\, d_n[t]^4}{\delta_n[t]\, P_n^{\text{tx}}}, \tag{2}$$

where κ_s absorbs wavelength, bandwidth, antenna gain, target radar cross-section (RCS), noise figure, and noise power [1]. Moreover, the range measurement Jacobian with respect to the target state is:

$$\mathbf{h}_n[t] = \left[\frac{\left(\mathbf{q}_n[t] - \boldsymbol{\xi}[t]\right)^T}{d_n[t]},\ \mathbf{0}_{1\times 3} \right] \in \mathbb{R}^{1\times 6}. \tag{3}$$

4) PCRB: The per-slot Fisher information contribution from MUAV n is:

$$\mathbf{J}_{M,n}[t] = \frac{1}{\sigma_n^2[t]}\, \mathbf{h}_n[t]^T \mathbf{h}_n[t]. \tag{4}$$

Let $\mathbf{J}[t] \in \mathbb{R}^{6\times 6}$ denote the cooperative Fisher information matrix (FIM) at slot t, whose inverse $\mathbf{J}[t]^{-1}$ is the PCRB on $\boldsymbol{\zeta}[t]$, as the lower bound on estimation error. $\mathbf{J}[t]$ is updated recursively as [2]:

$$\mathbf{J}[t] = \underbrace{\Big(\mathbf{F}\,\mathbf{J}[t-1]^{-1}\mathbf{F}^T + \mathbf{Q}\Big)^{-1}}_{\mathbf{J}_p[t]} + \sum_{n=1}^{N} \mathbf{J}_{M,n}[t], \quad (5)$$

where $\mathbf{J}_p[t]$ is the *prediction FIM* propagated from slot $t-1$. with $\mathbf{J}[0] = \mathbf{J}_0$ as the prior FIM. The sensing performance metric at slot t is the trace of the PCRB matrix:

$$\rho_t = \mathrm{tr}\big(\mathbf{J}[t]^{-1}\big)\,. \quad (6)$$

Note that ρ_t couples MUAV positions, sensing time fractions, and transmit powers through (2)–(4), and that geometric diversity among MUAVs (angular spread around the target) directly reduces ρ_t via the FIM structure.

5) Uplink Communication Model: The LoS-dominant air-to-ground channel gain from MUAV n to the BS is:

$$h_n[t] = \frac{\beta_0}{\|\mathbf{q}_n[t] - \mathbf{q}_{\rm bs}\|^2}, \quad (7)$$

where β_0 is the reference channel gain at 1 m. The achievable uplink rate during the communication phase is:

$$R_n[t] = (1-\delta_n[t])\,B\log_2\!\left(1 + \frac{P_n^{\rm tx}\,h_n[t]}{\sigma^2}\right), \quad (8)$$

where B is the allocated bandwidth and σ^2 is noise power.

C. Energy and Wireless Power Transfer Model

1) Propulsion Power: Both MUAVs and CUAVs are rotary-wing UAVs. The propulsion power as a function of horizontal speed v follows the standard model [12]:

$$P^{\rm prop}(v) = P_0\left(1 + \frac{3v^2}{V_{\rm tip}^2}\right) + P_1\sqrt{\sqrt{1+\frac{v^4}{4v_h^4}} - \frac{v^2}{2v_h^2}} + \tfrac{1}{2}\,d_0\,\rho_a\,s_r\,A\,v^3, \quad (9)$$

where P_0, P_1, $V_{\rm tip}$, v_h, d_0, ρ_a, s_r, and A are aerodynamic constants.

2) MUAV Battery Dynamics: Let $B_n[t]$ denote the SoC of MUAV n at the start of slot t. It evolves as:

$$B_n[t+1] = B_n[t] - \big(P^{\rm prop}(v_n[t]) + P_n^{\rm tx}\big)\tau + \zeta\sum_{m\in\mathcal{M}} a_{n,m}[t]\,p_{n,m}[t]\,\tau, \quad (10)$$

where $v_n[t] = \|\mathbf{q}_n[t+1] - \mathbf{q}_n[t]\|/\tau$ is the MUAV speed, $a_{n,m}[t] \in \{0,1\}$ is the *charging admission indicator* (CUAV m charges MUAV n), $p_{n,m}[t] \geq 0$ is the WPT transmit power from CUAV m, and $\zeta \in (0,1)$ is the end-to-end WPT efficiency (accounting for beamforming, conversion, and path losses at proximity range $d_{\rm wpt}$).

3) CUAV Battery Dynamics: Let $B_m^c[t]$ denote the SoC of CUAV m. CUAVs harvest ambient energy (e.g., solar irradiance) at power $e_m[t] \geq 0$ and spend energy on propulsion and WPT transmission:

$$B_m^c[t+1] = B_m^c[t] + e_m[t]\,\tau - P^{\rm prop}(v_m^c[t])\,\tau - \sum_{n\in\mathcal{N}} a_{n,m}[t]\,p_{n,m}[t]\,\tau, \quad (11)$$

where $v_m^c[t] = \|\mathbf{u}_m[t+1] - \mathbf{u}_m[t]\|/\tau$.

D. Problem Formulation

The optimization problem over the joint variable set $\mathbf{\Phi} = \{\mathbf{q}_n[t],\ \mathbf{u}_m[t],\ \delta_n[t],\ a_{n,m}[t],\ p_{n,m}[t]\}_{n,m,t}$ is:

$$(\mathbf{P}) : \min_{\mathbf{\Phi}} \quad \frac{1}{T}\sum_{t=1}^{T}\rho_t \quad (12a)$$

s.t.

$$R_n[t] \geq R_{\rm th}, \quad \forall n,\, t, \quad (C1)$$
$$0 \leq B_n[t] \leq B_n^{\max}, \quad \forall n,\, t, \quad (C2)$$
$$0 \leq B_m^c[t] \leq B_m^{c,\max}, \quad \forall m,\, t, \quad (C3)$$
$$a_{n,m}[t] \in \{0,1\}, \quad \forall n,\, m,\, t, \quad (C4a)$$
$$\textstyle\sum_n a_{n,m}[t] \leq 1, \quad \forall m,\, t, \quad (C4b)$$
$$\textstyle\sum_m a_{n,m}[t] \leq 1, \quad \forall n,\, t, \quad (C4c)$$
$$0 \leq p_{n,m}[t] \leq a_{n,m}[t]\,P_{\rm wpt}^{\max}, \quad \forall n,\, m,\, t, \quad (C5a)$$
$$a_{n,m}[t](\|\mathbf{q}_n[t] - \mathbf{u}_m[t]\| - d_{\rm wpt}) \leq 0,\ \forall n,\, m,\, t, \quad (C5b)$$
$$\|\mathbf{q}_n[t+1] - \mathbf{q}_n[t]\| \leq v_{\max}^m\tau, \quad \forall n,\, t, \quad (C6a)$$
$$\|\mathbf{u}_m[t+1] - \mathbf{u}_m[t]\| \leq v_{\max}^c\tau, \quad \forall m,\, t, \quad (C6b)$$
$$\|\mathbf{q}_n[t] - \mathbf{q}_{n'}[t]\| \geq d_{\rm safe}, \quad \forall n{\neq}n',\, t, \quad (C7a)$$
$$\|\mathbf{u}_m[t] - \mathbf{u}_{m'}[t]\| \geq d_{\rm safe}, \quad \forall m{\neq}m',\, t, \quad (C7b)$$
$$\delta_n[t] \in [0,1], \quad \forall n,\, t. \quad (C8)$$

The constraints encode the following requirements. **(C1)** guarantees *a minimum uplink rate* $R_{\rm th}$ for sensing-data delivery to the BS at every slot. **(C2)–(C3)** enforce *energy causality* for both tiers: MUAVs must not over-discharge (preserving operational capability) nor overcharge (preventing thermal damage), and CUAVs must not transmit more energy than they store. The upper bound in (C2) captures thermal charging-rate limits, complementing the WPT power cap in (C5a). **(C4a)–(C4c)** define *charging admission*: each CUAV may charge at most one MUAV per slot (C4b) and each MUAV may receive from at most one CUAV (C4c), forming a per-slot one-to-one assignment. **(C5a)–(C5b)** couple *WPT scheduling* to proximity: a non-zero $p_{n,m}[t]$ is only feasible when $a_{n,m}[t] = 1$, and charging is only admitted when the inter-UAV distance is within the WPT range $d_{\rm wpt}$. **(C6a)–(C6b)** and **(C7a)–(C7b)** enforce speed limits and *collision-free flight* for all intra-tier UAV pairs, respectively. **(C8)** bounds the sensing-communication time split.

Remark 1 (Problem Classification)**.** ***(P)*** *is a non-convex MIP due to (i) binary admission variables in* (C4a)*, (ii) non-convex*

PCRB objective in (12a) *coupling positions and time splits, (iii) bilinear WPT coupling in the battery dynamics* (10)–(11)*, (iv) non-convex collision constraints* (C7a)–(C7b)*, and (v) temporal coupling across slots via* (5) *and battery recursions.*

Remark 2 (Novelty Over Prior Art)**.** *Existing ISAC-UAV works [1], [2] minimize the PCRB but treat UAV energy as unlimited. WPT-assisted UAV works [5], [6] model battery dynamics but lack an ISAC sensing objective.* ***(P)*** *jointly optimizes cooperative ISAC trajectory planning (through* $\mathbf{q}_n$*,* δ_n*, and the cooperative PCRB* (5)*), U2U WPT scheduling (*$p_{n,m}$*) with per-slot admission (*$a_{n,m}$*), and dual-tier energy causality* (C2)–(C3) *for both mission and charging agents under a unified objective.*

III. Proposed Method

To solve Problem (12), we propose *receding-horizon alternating optimization (AO)* (RHAO): at each slot t, the current FIM $\mathbf{J}[t]$, battery states $(B_n[t], B^{c}_m[t])$, and the extended Kalman filter (EKF) one-step-ahead position estimate $\hat{\boldsymbol{\xi}}[t] = [\mathbf{F}\hat{\boldsymbol{\zeta}}[t-1]]_{1:3}$ serve as known initial conditions, and the slot's decision variables $\boldsymbol{\Phi}[t]$ are obtained by cycling over four tractable blocks until convergence, using the prediction FIM $\mathbf{J}_p[t]$ defined in (5).

A. Block 1 — Charging Admission

A MUAV n is declared *energy-critical* when its SoC falls below the trigger threshold $B_n^{\mathrm{trig}} \in (0, B_n^{\max})$, a design parameter set as a fraction of battery capacity to allow sufficient rendezvous time before depletion; this yields the candidate set $\mathcal{N}_c[t] = \{n : B_n[t] < B_n^{\mathrm{trig}}\}$. The binary one-to-one assignment satisfying (C4a)–(C4c) is obtained as a minimum-cost bipartite matching:

$$\{a^*_{n,m}\} = \underset{a_{n,m}\in\{0,1\}}{\arg\min} \sum_{n\in\mathcal{N}_c, m\in\mathcal{M}} a_{n,m}\|\mathbf{q}_n[t-1] - \mathbf{u}_m[t-1]\|, \tag{13}$$

with $a_{n,m} = 0$ for $n \notin \mathcal{N}_c[t]$, solved in closed form by the Hungarian algorithm [13]. Unassigned CUAVs maintain their last position.

B. Block 2 — MUAV Trajectory and Time-Split

1) Optimal time-split (closed form): For fixed MUAV positions, the objective ρ_t is strictly decreasing in each $\delta_n[t]$: more sensing time yields tighter range measurements (lower σ_n^2) and a larger FIM. The rate constraint (C1) therefore binds at the optimum, giving

$$\delta_n^*[t] = \left[1 - \frac{R_{\mathrm{th}}}{B\log_2\!\left(1 + \dfrac{P_n^{\mathrm{tx}}\beta_0}{\sigma^2\|\mathbf{q}_n[t]-\mathbf{q}_{\mathrm{bs}}\|^2}\right)}\right]_0^1, \tag{14}$$

where $[\,\cdot\,]_0^1$ denotes projection onto $[0,1]$. Each MUAV thus allocates the maximum feasible fraction of the slot to sensing while guaranteeing the uplink data delivery.

2) SCA trajectory update: With $\{\delta_n^*[t]\}$ fixed, Block 2 reduces to

$$\min_{\{\mathbf{q}_n[t]\}} \ \rho_t \quad \text{s.t.} \quad \text{(C6a), (C7a).} \tag{15}$$

The non-convexities are the PCRB objective and the collision constraints (C7a). We resolve both via successive convex approximation (SCA), iterating over position iterates $\{\mathbf{q}_n^{(l)}\}$, where l is the inner SCA loop iteration at each slot.

a) PCRB surrogate.: The objective $\rho_t = \mathrm{tr}(\mathbf{J}[t]^{-1})$ is non-convex in $\{\mathbf{q}_n\}$. To make it tractable we replace it with a *first-order Taylor surrogate* around the current iterate $\{\mathbf{q}_n^{(l)}\}$, which is linear in $\{\mathbf{q}_n\}$ and therefore convex. Let $\mathbf{J}^{(l)} = \mathbf{J}_p[t] + \sum_n \mathbf{J}_{M,n}(\mathbf{q}_n^{(l)}, \delta_n^*)$, $\boldsymbol{\Psi}^{(l)} = (\mathbf{J}^{(l)})^{-1}$, and $\mathbf{e}_n^{(l)} = \mathbf{q}_n^{(l)} - \hat{\boldsymbol{\xi}}[t]$. The first-order Taylor expansion of ρ_t around $\{\mathbf{q}_n^{(l)}\}$ is

$$\rho_t \approx \rho_t^{(l)} + \sum_{n=1}^{N}\big(\nabla_{\mathbf{q}_n}\rho_t\big)^T\big(\mathbf{q}_n - \mathbf{q}_n^{(l)}\big), \tag{16}$$

where $\rho_t^{(l)}$ and $\mathbf{q}_n^{(l)}$ are constants at iteration l. Substituting $\mathbf{w}_n^{(l)} = -\nabla_{\mathbf{q}_n}\rho_t\big|_{\mathbf{q}_n^{(l)}}$ and absorbing all constant terms into $c^{(l)}$ reduces (16) to the PCRB surrogate:

$$\tilde{\rho}^{(l)}\big(\{\mathbf{q}_n\}\big) = c^{(l)} - \sum_{n=1}^{N}\big(\mathbf{w}_n^{(l)}\big)^T\mathbf{q}_n, \tag{17}$$

where $\mathbf{w}_n^{(l)}$ is the *sensing gradient*; the direction in which moving MUAV n most reduces ρ_t locally. To compute $\mathbf{w}_n^{(l)}$, note that only $\mathbf{J}_{M,n}$ depends on $\mathbf{q}_n$; the chain rule with the identity $\nabla_{\mathbf{J}}\mathrm{tr}(\mathbf{J}^{-1}) = -(\boldsymbol{\Psi}^{(l)})^2$ reduces the problem to differentiating $\mathbf{J}_{M,n} = (c_n/{d_n^{(l)}}^6)\,\mathbf{e}_n^{(l)}{\mathbf{e}_n^{(l)}}^T$ with respect to $\mathbf{q}_n$. Applying the product rule and letting $\mathbf{A}^{(l)} = \big[(\boldsymbol{\Psi}^{(l)})^2\big]_{1:3,1:3}$ gives:

$$\mathbf{w}_n^{(l)} = \frac{2c_n}{{d_n^{(l)}}^6}\left[\mathbf{A}^{(l)}\mathbf{e}_n^{(l)} - \frac{3\,{\mathbf{e}_n^{(l)}}^T\mathbf{A}^{(l)}\mathbf{e}_n^{(l)}}{{d_n^{(l)}}^2}\,\mathbf{e}_n^{(l)}\right], \tag{18}$$

with $c_n = \delta_n^* P_n^{\mathrm{tx}}/\kappa_s$ and $d_n^{(l)} = \|\mathbf{e}_n^{(l)}\|$. Minimizing (17) moves each MUAV along $\mathbf{w}_n^{(l)}$, balancing proximity to the target (via d_n^{-6}) and cooperative geometric diversity (via $\mathbf{A}^{(l)}$).

b) Collision constraint linearization.: The non-convex constraint (C7a) is replaced by its first-order lower bound at the current iterate. Letting $\mathbf{d}_{nn'}^{(l)} = \mathbf{q}_n^{(l)} - \mathbf{q}_{n'}^{(l)}$:

$$2\,{\mathbf{d}_{nn'}^{(l)}}^T(\mathbf{q}_n - \mathbf{q}_{n'}) \geq d_{\mathrm{safe}}^2 + \|\mathbf{d}_{nn'}^{(l)}\|^2, \quad \forall\, n \neq n'. \tag{19}$$

The per-SCA-iteration sub-problem–linear objective (17), second-order cone speed constraints (C6a), and affine collision constraints (19)–is a second-order cone program (SOCP) solvable in polynomial time by standard convex solvers (e.g., CVX/MOSEK [14]).

Algorithm 1 RHAO — Receding-Horizon Alternating Optimization

Require: Initial positions $\mathbf{q}_n[0], \mathbf{u}_m[0]$; $\mathbf{J}[0] = \mathbf{J}_0$; batteries $B_n[0], B_m^{\mathrm{c}}[0]$; B_n^{trig}; tolerance $\epsilon > 0$.

for $t = 1, 2, \ldots, T$ **do**
- **EKF predict (state):** $\hat{\boldsymbol{\xi}}[t] \leftarrow [\mathbf{F}\hat{\boldsymbol{\zeta}}[t-1]]_{1:3}$.
- **EKF predict (FIM):** $\mathbf{J}_p[t] \leftarrow (\mathbf{F}\mathbf{J}[t-1]^{-1}\mathbf{F}^T + \mathbf{Q})^{-1}$.
- **Block 1:** Solve (13) via Hungarian $\rightarrow \{a_{n,m}^*\}$.
- **Block 2:** Initialize $\mathbf{q}_n^{(0)} \leftarrow \mathbf{q}_n[t-1]$, $l \leftarrow 0$.
- **repeat**
  - Compute δ_n^* via (14) at $\mathbf{q}_n^{(l)}$.
  - Compute $\boldsymbol{\Psi}^{(l)}, \mathbf{A}^{(l)}, \{\mathbf{w}_n^{(l)}\}$ via (18).
  - Solve SOCP $((17), (\text{C6a}), (19)) \rightarrow \{\mathbf{q}_n^{(l+1)}\}$.
  - $l \leftarrow l + 1$.
- **until** $|\tilde{\rho}^{(l)} - \tilde{\rho}^{(l-1)}| \leq \epsilon$
- $\mathbf{q}_n[t] \leftarrow \mathbf{q}_n^{(l)}$; $\delta_n[t] \leftarrow \delta_n^*$.
- **Block 3:** Compute $\mathbf{u}_m^*[t]$ via (20).
- **Block 4:** Compute $p_{n,m}^*[t]$ via (21).
- Execute decisions; take radar measurements.
- Update PCRB via (5); update batteries via (10)–(11).
- **EKF update:** incorporate range measurements (2) $\rightarrow \hat{\boldsymbol{\zeta}}[t]$.

end for

C. Block 3 — CUAV Rendezvous Trajectory

Each assigned CUAV m ($a_{n,m}^* = 1$) flies at maximum speed toward its paired MUAV subject to (C6b):

$$\mathbf{u}_m^*[t] = \mathbf{u}_m[t-1] + \min\big(v_{\max}^c \tau,\, d_{nm}[t]\big)\, \hat{\mathbf{d}}_{nm}[t], \qquad (20)$$

where $d_{nm}[t] = \|\mathbf{q}_n[t] - \mathbf{u}_m[t-1]\|$ and $\hat{\mathbf{d}}_{nm}[t]$ is the unit direction vector. Unassigned CUAVs hover. Inter-CUAV conflicts (C7b) are resolved by a priority rule: the CUAV serving the more energy-critical MUAV proceeds; the other holds position for one slot.

D. Block 4 — WPT Power Allocation

Let $d_{nm}[t] = \|\mathbf{q}_n[t] - \mathbf{u}_m^*[t]\|$ and $\bar{p}_{nm}[t] = \min(P_{\mathrm{wpt}}^{\max}, B_m^c[t]/\tau)$ denote the inter-pair distance and the battery-capped power ceiling, respectively. WPT is active only when admitted and within proximity range; the power satisfying (C3)–(C5b) is:

$$p_{n,m}^*[t] = \begin{cases} \bar{p}_{nm}[t] & \text{if } a_{n,m}^*[t] = 1 \;\&\; d_{nm}[t] \leq d_{\mathrm{wpt}}, \\ 0 & \text{otherwise.} \end{cases} \qquad (21)$$

E. Overall Algorithm and Convergence

Algorithm 1 summarizes RHAO. The dominant per-slot cost is the SOCP in Block 2: with $3N$ position variables and $\binom{N}{2}$ linearized collision constraints, each SCA iteration has complexity $\mathcal{O}(N^{3.5})$; in practice, the inner loop converges in 5–10 iterations.

Remark 3 (Convergence)**.** *Each SCA iterate produces a feasible point with $\tilde{\rho}^{(l+1)} \leq \tilde{\rho}^{(l)}$; since $\tilde{\rho}$ is bounded below by zero, the inner loop converges [15]. The outer AO loop over Blocks 1–4 inherits monotone non-increase of ρ_t per outer iteration.*

IV. Simulation Results

A. Setup

We simulate a $1\,\mathrm{km} \times 1\,\mathrm{km}$ area over $T{=}60$ slots of $\tau{=}1\,\mathrm{s}$ each, with $N{=}3$ MUAVs and $M{=}2$ CUAVs fixed at altitude $H{=}100\,\mathrm{m}$. The ground BS is placed at the origin. A single aerial target at altitude $50\,\mathrm{m}$ moves under a near-constant-velocity model (1) with initial position $(300, 300)\,\mathrm{m}$ and velocity $(7, 4)\,\mathrm{m/s}$ (process noise $\sigma_q{=}0.5\,\mathrm{m/s^2}$). MUAVs are initialized in an equilateral triangle of radius $150\,\mathrm{m}$ centred on the target's initial position, providing a well-diversified sensing geometry from the outset. Key ISAC parameters are: $\kappa_s{=}5{\times}10^{-9}$, $P_n^{\mathrm{tx}}{=}1\,\mathrm{W}$, $B{=}10\,\mathrm{MHz}$, $\beta_0{=}10^{-4}$, $\sigma^2{=}4{\times}10^{-13}\,\mathrm{W}$, and $R_{\mathrm{th}}{=}1\,\mathrm{Mbps}$. Kinematic limits are $v_{\max}^m{=}25\,\mathrm{m/s}$, $v_{\max}^c{=}20\,\mathrm{m/s}$, and $d_{\mathrm{safe}}{=}20\,\mathrm{m}$. Each MUAV starts with $B_n^{\mathrm{init}}{=}12\,\mathrm{kJ}$ out of a $20\,\mathrm{kJ}$ capacity; CUAVs start with $60\,\mathrm{kJ}$ out of $80\,\mathrm{kJ}$ and harvest $200\,\mathrm{W}$ of solar power continuously. The WPT proximity radius is $d_{\mathrm{wpt}}{=}50\,\mathrm{m}$, the maximum transmit power is $P_{\mathrm{wpt}}^{\max}{=}500\,\mathrm{W}$ at efficiency $\zeta{=}0.8$, and the energy-critical trigger threshold is $B_n^{\mathrm{trig}}{=}6\,\mathrm{kJ}$. All results are averaged over 10 Monte-Carlo runs.

B. Baselines

We compare RHAO against four reference schemes, ordered from structurally closest to most naive:

- **B1-Static (Wang et al. [2]):** MUAVs are held at their initial positions throughout the mission. The optimal time split δ_n^* (14) is applied slot-by-slot, and CUAVs use nearest-neighbour WPT admission. This isolates the gain due to *trajectory optimization* in RHAO.
- **B2-Fixed-δ Greedy (Li et al. [3]):** Each MUAV flies at maximum speed toward the current target estimate, but uses a *fixed* time split $\delta_n{=}0.5$ (uniform time division). This isolates the gain due to *joint time-split optimization* in RHAO.
- **B3-Pure Greedy:** Each MUAV flies toward the target estimate with the optimal time split δ_n^* and collision-avoidance deflection, but trajectory decisions are made greedily per MUAV without SCA. This isolates the value of the *convex trajectory subproblem* in RHAO.
- **B4-Random:** MUAVs select uniformly random headings and speeds; δ_n is sampled from $\mathcal{U}(0, 1)$; WPT pairs are random. This provides a lower bound on performance.

C. Results

Sensing quality (Fig. 2a). All methods begin at the same prior $\rho_1 \approx 80\,\mathrm{m}^2$ (determined by $\mathbf{J}_0$) and improve as measurements accumulate. RHAO reaches $\rho_t \approx 1\,\mathrm{m}^2$ by slot 5 and sustains sub-$10\,\mathrm{m}^2$ performance throughout most of the horizon, yielding a mean of $\bar{\rho}^{\mathrm{RHAO}} = 74.5\,\mathrm{m}^2$ (driven by the transient at slot 1 and a late-episode rise as battery constraints bite around slot 50). **B1-Static** drops to $\approx 10\,\mathrm{m}^2$ while the target remains near the initial formation, but degrades monotonically to $\approx 10^3\,\mathrm{m}^2$ as the target moves away ($\bar{\rho} = 400.6$, $5.4\times$ worse than RHAO). **B3-Pure Greedy** achieves a similar low early, but without SCA coordination it loses angular diversity

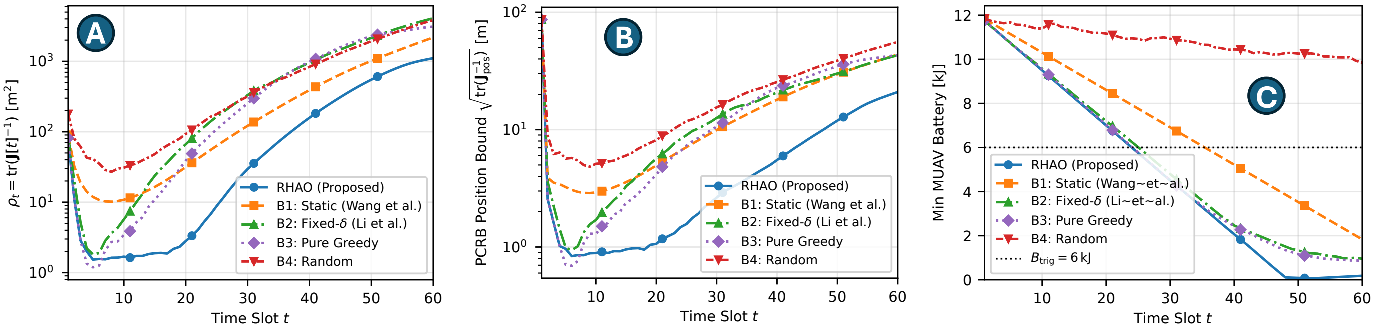

Fig. 2. Simulation results averaged over 10 Monte-Carlo runs. **(a)** Sensing quality: $\rho_t = \mathrm{tr}(\mathbf{J}[t]^{-1})$ vs. slot (log scale). **(b)** Tracking accuracy: PCRB position bound $\sqrt{\mathrm{tr}(\mathbf{J}_{\mathrm{pos}}^{-1})}$ vs. slot (log scale). **(c)** Energy sustainability: minimum MUAV battery vs. slot; dashed line marks the energy-critical trigger B_n^{trig}=6 kJ (Block 1 admission threshold).

after roughly 20 slots and degrades sharply ($\bar{\rho} = 644.8$). **B2-Fixed-δ** suffers from under-utilized sensing time: fixing δ=0.5 sacrifices up to 40% of the achievable FIM contribution per slot, resulting in $\bar{\rho} = 1246.8$ (16.8× worse), the worst among all baselines. **B4-Random** is close behind ($\bar{\rho} = 1204.6$).

Tracking accuracy (Fig. 2b). The PCRB position bound $\sqrt{\mathrm{tr}(\mathbf{J}_{\mathrm{pos}}^{-1})}$, where $\mathbf{J}_{\mathrm{pos}}$ is the 3×3 position-state subblock of $\mathbf{J}[t]^{-1}$, mirrors the sensing quality trend. RHAO maintains a mean position RMSE bound of 4.5 m, compared to 15.4 m for B1-Static and 22.3 m for B2-Fixed-δ, confirming that active tracking and adaptive time-split are both essential.

Energy sustainability (Fig. 2c). RHAO consumes the most energy per slot (active trajectory requires propulsion), yet CUAV WPT sustains all MUAVs above B_n^{trig} for the T=60 horizon. Static and random baselines conserve battery (B1 hovering, B4 low speed) but sacrifice sensing quality. This validates receding-horizon optimization with aerial WPT: RHAO achieves the best sensing performance while keeping MUAVs energized for the full mission.

V. Conclusion

This paper proposed a two-tier UAV swarm architecture for mission-critical ISAC, where MUAVs performed cooperative aerial target tracking while solar-powered CUAVs provided aerial WPT to sustain energy continuity. The joint optimization of trajectories, sensing–communication time splits, and WPT scheduling was formulated as a non-convex MIP minimizing the cooperative PCRB, and solved via the proposed RHAO algorithm using SCA and the Hungarian method. Simulations showed that RHAO reduced the mean PCRB by 16.8× over a fixed-time-split baseline and 5.4× over a static-trajectory scheme, while sustaining all MUAVs above the energy-critical threshold throughout the full mission. Future work will explore extending the framework to multiple simultaneous targets and heterogeneous sensing modalities, as well as incorporating learning-based trajectory policies [16] to further reduce per-slot computational overhead.

Acknowledgment

This work was, in part, supported by BMFTR, Germany (6GEM+, Grant 16KIS2411), and the EU Horizon Europe programme (6G-Path, Grant 101139172).

References

[1] K. Yan *et al.*, "Curriculum-Guided Heterogeneous Multi-Agent Intelligence for Multi-UAV Cooperative ISAC," *IEEE Transactions on Communications*, pp. 1–1, 2026.

[2] R. Wang *et al.*, "ISAC-Enabled Multi-UAV Collaborative Target Sensing for Low-Altitude Economy," Mar. 2026, arXiv:2603.11502 [eess.SY].

[3] F. Li *et al.*, "Cooperative ISAC for LAE: Joint Trajectory Planning, Power allocation, and Dynamic Time Division," Apr. 2026, arXiv:2511.13006 [eess.SY].

[4] Z. Feng *et al.*, "ISAC-Enabled Deep RL-Based UAV 3D Trajectory Design for Urban Relaying with User Tracking," in *GLOBECOM 2025 - 2025 IEEE Global Communications Conference*, Dec. 2025, pp. 2270–2275, iSSN: 2576-6813.

[5] U. Naoya *et al.*, "Multi-UAV Data Collection with In-Flight Wireless Power Transfer," in *2025 IEEE VTS Asia Pacific Wireless Communications Symposium (APWCS)*, Aug. 2025, pp. 1–3.

[6] Q. Zhang *et al.*, "eU2U: Energy-Efficient Wireless Charging and Trajectory Design for IoT Data Collection," in *2025 IEEE 22nd Consumer Communications & Networking Conference (CCNC)*, Jan. 2025, pp. 1–6, iSSN: 2331-9860.

[7] M. S. Mondal *et al.*, "Risk-Aware Energy-Constrained UAV-UGV Cooperative Routing Using Attention-Guided Reinforcement Learning," in *2025 IEEE International Conference on Robotics and Automation (ICRA)*, May 2025, pp. 13 000–13 006.

[8] Y. Ye *et al.*, "Multi-Tier UAV Edge Computing Towards Long-Term Energy Stability for Low Altitude Networks," Feb. 2026, arXiv:2602.04258.

[9] K. Gao *et al.*, "LE-MHAPPO-Enhanced DNN Task Partitioning in Energy-Harvesting Heterogeneous UAV Swarms," in *ICC 2025 - IEEE International Conference on Communications*, Jun. 2025, pp. 1280–1285, iSSN: 1938-1883.

[10] M. Farhoudi *et al.*, "Energy efficient orchestration in multiple-access vehicular aerial-terrestrial 6G networks," *IEEE Transactions on Vehicular Technology*, pp. 1–16, 2026.

[11] M. Farhoudi *et al.*, "Multi-agent reinforcement learning for SLA-aware network slicing in UAV-enabled MEC," Jul. 2026, arXiv:2607.09295.

[12] Y. Zeng *et al.*, "Energy minimization for wireless communication with rotary-wing UAV," *IEEE Transactions on Wireless Communications*, vol. 18, no. 4, pp. 2329–2345, Apr. 2019.

[13] H. W. Kuhn, "The Hungarian method for the assignment problem," *Naval Research Logistics Quarterly*, vol. 2, no. 1–2, pp. 83–97, 1955.

[14] M. Grant *et al.*, "CVX: Matlab software for disciplined convex programming, version 2.1," http://cvxr.com/cvx, 2014.

[15] M. Razaviyayn *et al.*, "A unified convergence analysis of block successive minimization methods for nonsmooth optimization," *SIAM Journal on Optimization*, vol. 23, no. 2, pp. 1126–1153, 2013.

[16] M. Farhoudi *et al.*, "Quality-aware personalized AI service provisioning in UAV-assisted 6G networks," Jul. 2026, arXiv:2607.06278.